This is a preprint, the final version is subject to change, of the American Mineralogist (MSA)
Cite as Authors (Year) Title. American Mineralogist, in press.
DOI: https://doi.org/10.2138/am-2018-6480

Revision 1 (#6480):

Pressure, temperature, water content, and oxygen fugacity dependence of Mg grain-boundary diffusion coefficient in forsterite

Authors:

Hongzhan Fei[1,2]*, Sanae Koizumi[3], Naoya Sakamoto[4], Minako Hashiguchi[5,a], Hisayoshi Yurimoto[4,5], Katharina Marquardt[1], Nobuyoshi Miyajima[1], Tomoo Katsura[1]

[1]Bayerisches Geoinstitut, University of Bayreuth, Bayreuth D95440, Germany

[2]Institute for Study of the Earth's Interior, Okayama University, Misasa, Tottori 6820193, Japan

[3]Earthquake Research Institute, University of Tokyo, 1-1-1 Yayoi, Tokyo, 1130032 Japan

[4]Isotope Imaging Laboratory, Creative Research Institution, Hokkaido University, Sapporo 0010021, Japan

[5]Department of Natural History Sciences, Hokkaido University, Sapporo, 0600810, Japan

[a]Present address: Research Center for Planetary Trace Organic Compounds, Kyushu University, Motooka, Nishi-ku, Fukuoka, 8190395, Japan

*Corresponding author: H. Fei (hongzhan.fei@uni-bayreuth.de). Bayerisches Geoinstitut, University of Bayreuth, Bayreuth D95440, Germany

Abstract:

Mg grain boundary diffusion coefficients were measured in forsterite aggregates as a function of pressure (1 atm - 13 GPa), temperature (1100 – 1300 K), water content (<1 – 350 wt. ppm bulk water), and oxygen fugacity (10^{-18} – $10^{-0.7}$ bar) using multi-anvil apparatus and gas-mixing furnace. The diffusion profiles were analyzed by secondary ion mass spectrometer, whereas the water contents in the samples were measured by Fourier transform infrared spectrometer. The activation volume, activation enthalpy, water content exponent, and oxygen fugacity exponent for the Mg grain-boundary diffusion coefficients are found to be 3.9 ± 0.7 cm^3/mol, 355 ± 25 kJ/mol, 1.0 ± 0.1, and -0.02±0.01, respectively. By comparison with the Mg lattice diffusion data (Fei et al. 2018), the bulk diffusivity of Mg in forsterite is dominated by lattice diffusion if the grain size is larger than ~1 mm under upper mantle conditions, whereas effective grain-boundary and lattice diffusivities are comparable when the grain size is ~1 – 100 μm.

Key words:

Mg grain-boundary diffusion; forsterite; upper mantle.

1. Introduction

$(Mg,Fe)_2SiO_4$ olivine is one of the most important minerals, which constitutes about 60 vol.% of the Earth's upper mantle (Ringwood 1991), and forsterite is the Mg-rich endmember of olivine (Fo100-90). Measurements of atomic diffusivities in forsterite are therefore important for understanding various mineral properties such as ionic electrical conductivity, rheology, crystal

growth, chemical equilibration, and kinetics of mass transfer, all of which are active participants of mantle dynamics.

Magnesium is the fastest major element diffusing in forsterite (e.g., Chakraborty et al. 1994; Farver et al. 1994; Fei et al. 2018). Mg diffusivity in forsterite can provide fundamental constraints for ionic conductivity (Fei et al. 2018). Since atomic diffusion occurs both within the crystal lattice and along the grain-boundaries, measurements of both the lattice and grain-boundary diffusion coefficients (D_{Mg}^{lat} and D_{Mg}^{gb}, respectively) are required. Chakraborty et al. (1994) and Farver et al. (1994), respectively, measured D_{Mg}^{lat} and D_{Mg}^{gb} in anhydrous forsterite as a function of temperature at ambient pressure. However, it should be more essential to measure them under hydrous conditions since 1) the Earth's upper mantle contains 10^1-10^4 wt. ppm water (e.g., Dixon et al. 2002; Workman and Hart, 2005); and 2) even tiny amounts of water (at wt. ppm level) may significantly enhance atomic diffusivity, at least lattice diffusivity, as demonstrated by Costa and Chakraborty (2008) and Fei et al. (2018).

Here we report the experimental grain boundary diffusion coefficient of Mg obtained in fine-grained iron-free forsterite aggregates (Fo100) as functions of pressure (1-atm, 1, 4, 8, and 13 GPa), for a limited temperature range (1100-1300 K), bulk water content (C_{H2O}^{bulk}) from <1 to 350 wt. ppm, and an oxygen fugacity (f_{O2}) ranging from 10^{-18} to $10^{-0.7}$ bar (i.e., 10^{-22} to $10^{-4.7}$ GPa). We then compare our results to previously reported values of Mg diffusivity in the lattice of olivine and forsterite to constrain quantitatively ionic conduction in Earth's upper mantle.

2. Experimental methods

The experimental protocol used here is identical to the one reported by Fei et al. (2016, 2018) and is briefly reported here. Fine-grained Mg_2SiO_4-forsterite aggregates with grain size of about 0.6 μm were synthesized from SiO_2 and $Mg(OH)_2$ at 1630 K in a vacuum furnace at Earthquake Research Institute, the University of Tokyo (Koizumi et al. 2010). Several pieces of aggregates were further heated at 1700 K to yield a grain-size about 2.0 μm. In each Pt capsule, the fine-grained forsterite aggregates sample was associated with graphite + enstatite as an oxygen fugacity (f_{O2}) and silica activity buffer, respectively, and brucite + talc as water source. The capsule is then welded and annealed at 1 - 13 GPa, 1100 – 1300 K in a multi-anvil press at the University of Bayreuth for defect equilibrium (water equilibrium). Water contents in the samples were controlled by ratios of talc + brucite to graphite + enstatite (Table 1). For ambient-pressure experiments, the samples with enstatite buffer were loaded into a Pt capsule without welding and annealed at 1300 K in a CO-CO_2 gas-mixing furnace at 1 atm with f_{O2} ranging from 10^{-18} to $10^{-0.7}$ bar (10^{-22} to $10^{-4.7}$ GPa). Sequentially, the samples were polished, coated with 600-1000 nm thick amorphous ^{25}Mg-enriched Mg_2SiO_4, and annealed again for diffusion under the same experimental conditions and chemical environments as those for defect equilibrium anneals. The experimental conditions and resulting diffusion coefficients are listed in Table 1. The water contents in the samples before and after diffusion were analyzed by Fourier transmission infrared spectrometer (FTIR) at the University of Bayreuth. Diffusion profiles were obtained by CAMECA ims-6f secondary ion mass spectrometer (SIMS) at Hokkaido University. Scanning electron microprobe (SEM) and transmission electron microprobe (TEM) images of the recovered samples were given in Fig. 1 and Fei et al. (2016, 2018).

To investigate the effect of water on D_{Mg}^{gb}, we should identify and quantify the amount of water in the grain-boundaries via FTIR spectra. Here we applied two methods for the approaching. 1) the OH in olivine lattices and grain boundaries show as sharp peaks and broad bands in FTIR spectra, respectively (Keppler and Rauch, 2000), therefore the infrared absorption contributed by grain boundary OH (Abs^{gb}) were calculated by integration of the broad bands from 3000 to 4000 cm^{-1} (Fig. 2a). 2) the infrared absorptions observed at wavenumbers of 3613, 3579, 3568, 3550, 3473 cm^{-1} were assigned as lattice OH (e.g., Lemaire et al., 2004), after deconvolution of these peaks, Abs^{gb} were obtained by integration of the residual spectra from 3000 to 4000 cm^{-1} (Fig. 2b). Due to the lack of FTIR calibrations specified for water-derived species sitting along grain boundaries, we report D_{Mg}^{gb} as a function of Abs^{gb} instead of water content, although C_{H2O}^{bulk} were reported in Table 1 based on Withers et al. (2012)'s calibration by assuming the same absorption coefficient for lattice and grain boundary OH in iron-bearing olivine and pure forsterite.

The products of Mg grain-boundary diffusion coefficients and grain-boundary width (δ) were obtained by fitting the grain-boundary diffusion regimes of the diffusion profiles (Fig. 3) to the equation (Le Claire, 1963),

$$\delta D_{\mathrm{Mg}}^{\mathrm{gb}} = 0.66 \left(\frac{\partial \ln(c_x - c_0)}{\partial x^{6/5}}\right)^{-5/3} \left(\frac{4 D_{\mathrm{Mg}}^{\mathrm{lat}}}{t}\right)^{1/2} \qquad (1)$$

where x is the depth from the surface, c_x is the observed abundance of ^{25}Mg expressed by $^{25}Mg/(^{25}Mg+^{24}Mg)$ as a function of x measured by SIMS, c_0 is the initial abundance of ^{25}Mg in the

forsterite aggregates, t is the annealing duration, and D_{Mg}^{lat} is the lattice diffusion coefficient reported in Fei et al. (2018).

The effective bulk grain-boundary diffusivity ($D_{Mg}^{gb(bulk)}$) is defined by $\delta D_{Mg}^{gb}/3d$ (e.g., Balluffi et al. 2005; Harrison, 1961). Therefore, it is not necessary to calculate D_{Mg}^{gb} from δD_{Mg}^{gb} for estimation of the effective bulk diffusivity. Indeed, δ in iron-bearing olivine (Fo90) has been roughly estimated to be 1 nm at 1 atm, (e.g., Hiraga et al. 2002), and so far no quantification of the evolution of δ with hydrogen incorporation or increasing pressure has been reported, although it is found that there is no significant difference of δ among different minerals (Marquardt and Faul, 2018), and no evolution of grain boundary character distribution with increasing pressure (Marquardt et al., 2015).

3. Experimental results and discussions

3.1 Time series

Atomic diffusion in minerals is usually very slow (e.g., $D_{Mg}^{lat} \approx 10^{-19}$ m^2/s, $D_{Mg}^{gb} \approx 10^{-15}$ m^2/s in forsterite at 1300 K). Diffusion profiles obtained by laboratory experiments are therefore very short, typically within a few of microns (Chakraborty et al. 1994; Farver et al. 1994; Fei et al. 2018). Artificial results could be produced due to limited analytical resolution. To confirm the robustness of the results, we performed time-series experiments in which diffusion experiments were conducted under identical pressure, temperature, water content, and f_{O2} conditions, but at different annealing durations. With longer duration, the diffusion profile should be longer, whereas the fitting results of δD_{Mg}^{gb} should remain constant. As shown in Fei et al. (2018), the

diffusion profile of the sample with annealing duration of 10 h is considerably longer (slope is smaller) than that with 1 h; whereas δD_{Mg}^{gb} does not show annealing duration dependence (Fig. 4).

3.2 Pressure dependence

The δD_{Mg}^{gb} measured at a constant temperature of 1300 K under nominally anhydrous conditions is shown in Fig. 5. With increasing pressure from 1-atm to 13 GPa, δD_{Mg}^{gb} systematically decreases by about two orders of magnitude. Although the diffusion experiments at 1 atm and at 1 – 13 GPa were performed using different apparatus (gas-mixing furnace and multi-anvil apparatus, respectively), they show relatively consistent values of δD_{Mg}^{gb}. Namely, the systematic errors in the experiments are negligible.

It should also be noted that, FTIR spectra from these anhydrous condition samples do not show any peaks related to the OH bonding, the actual water contents of the samples at 1 atm should be much lower than those at high pressures of 1 – 13 GPa. Hence, the agreement between ambient and high-pressure experiments indicates that the effect of water on δD_{Mg}^{gb} is not significant when the water content is below the FTIR detection limit (1 wt. ppm).

The data points under anhydrous conditions are fitted to the pressure derivation of the Arrhenius equation,

$$\left(\frac{\partial \ln\left(\delta D_{Mg}^{gb}\right)}{\partial P}\right)_T = -\frac{\Delta V_{Mg}^{gb}}{RT} \quad (2)$$

where P is the pressure, T is the temperature, ΔV_{Mg}^{gb} is the activation volume for δD_{Mg}^{gb}, and R is ideal gas constant. The ΔV_{Mg}^{gb} is found to be 3.9 ± 0.7 cm^3/mol by least square fitting.

The ΔV_{Mg}^{gb} determined in this study is nearly identical to that for lattice diffusion in forsterite (ΔV_{Mg}^{lat} = 4.3 ± 0.3 cm^3/mol reported by Fei et al. (2018)) and similar as that calculated based on computational simulation (4.7 cm^3/mol reported by Béjina et al. (2009)), but significantly larger than that reported by Farver et al. (1994) who reported a value of ≤ 1.0 cm^3/mol. The δD_{Mg}^{gb} values under ambient pressure conditions determined by this study and by Farver et al. (1994) are in agreement, whereas the deviation increases with increasing pressure. We note that the samples in the high pressure experimental set up of Farver et al. (1994) were surrounded by NaCl, which may easily absorb moisture from the air during sample capsule preparation even though they dried it in prior to compression. Therefore, it is likely that their high-pressure samples contained some hydrogen incorporated in the forsterite samples. That could lead to apparent smaller ΔV_{Mg}^{gb} because incorporation of water significantly enhances the atomic diffusivity on the metal site (Fei et al. 2018; Hier-Majumder et al. 2005; Wang et al. 2004).

3.3 Temperature dependence

The temperature dependence of δD_{Mg}^{gb} in hydrous forsterite at various levels of C_{H2O}^{bulk} is shown in Fig. 6. With increasing temperature, δD_{Mg}^{gb} considerably increases. On the other hand, water significantly enhances the diffusion coefficients. Therefore, the diffusion coefficients under hydrous conditions are fitted to the Arrhenius equation including a water (infrared absorptions) exponent,

$$\delta D_{\mathrm{Mg}}^{\mathrm{gb}} = D_{\mathrm{Mg},0}^{\mathrm{gb}} \left(Abs^{\mathrm{gb}}\right)^{r^{\mathrm{gb}}} \exp\left(-\frac{\Delta H_{\mathrm{Mg}}^{\mathrm{gb}}}{RT}\right) \qquad (3)$$

where $D_{Mg,0}^{gb}$ is the pre-exponential factor, r^{gb} is the water content exponent for δD_{Mg}^{gb}, Abs^{gb} is the infrared absorptions contributed by grain boundary OH integrated from 3000 to 4000 cm^{-1},

and ΔH_{Mg}^{gb} is the activation enthalpy. By least square fitting, the $D_{Mg,0}^{gb}$, r^{gb}, and ΔH_{Mg}^{gb} are found to be $10^{-11.7\pm1.0}$ m^2/s, 1.0 ± 0.1, and 355 ± 25 kJ/mol, respectively, based on Abs^{gb} calculated from Fig. 2a, and $10^{-12.6\pm1.1}$ m^2/s, 1.0 ± 0.1, and 330 ± 30 kJ/mol, respectively, based on Abs^{gb} calculated from Fig. 2b.

Farver et al. (1994) reported the activation energy (ΔE_{Mg}^{gb}) of 343 ± 27 and 376 ± 47 kJ/mol for CO + CO_2 and H_2 + CO_2 buffered samples, respectively. Using the ΔV_{Mg}^{gb} determined in this study, the ΔH_{Mg}^{gb} at 8 GPa becomes 370-410 kJ/mol. It is slightly higher, but within the experimental error as that found in this study.

We note that, $\Delta H_{Mg}^{gb} \approx \Delta H_{Mg}^{lat}$ (ΔH_{Mg}^{gb} = 370-410 kJ/mol (Farver et al. 1994), ΔH_{Mg}^{lat} = 400 ± 60 kJ/mol (Chakraborty et al. 1994)) in anhydrous forsterite, but $\Delta H_{Mg}^{gb} >> \Delta H_{Mg}^{lat}$ (330~355 kJ/mol (this study) vs. 280 ± 30 kJ/mol (Fei et al. 2018)) under hydrous conditions. As we know, the activation energy for grain-boundary diffusion is usually much smaller than that for lattice diffusion, for example Si and O diffusion in forsterite, wadsleyite, and ringwoodite (Farver and Yund, 2000; Fei et al. 2012, 2013, 2016; Shimojuku et al. 2009), and H, He, Ar diffusion in olivine (Burnard et al., 2015; Demouchy and Mackwell 2006; Demouchy 2010). The exact reason for $\Delta E_{Mg}^{gb} >> \Delta E_{Mg}^{lat}$ in hydrous forsterite is unclear, here we propose the following scenario.

Diffusion can be dominated either by an intrinsic mechanism (controlled by intrinsic point defects formed by thermal activation), or by an extrinsic mechanism (controlled by extrinsic point defects formed by impurities such as H^+ and Fe^{3+}). A diffusion process dominated by an intrinsic mechanism usually has a higher activation energy than an extrinsic one because of additional energy required for defect formation (Chakraborty et al. 1994). The activation enthalpy for

178 intrinsic Mg diffusion is ~380 kJ/mol based on computational simulation (Béjina et al. 2009). It is
179 close to both ΔH_{Mg}^{gb} and ΔH_{Mg}^{lat} in anhydrous forsterite (Chakraborty et al. 1994; Farver et al.
180 1994). Therefore, both D_{Mg}^{lat} and D_{Mg}^{gb} under anhydrous conditions are expected to be controlled
181 by an intrinsic mechanism. Namely, the concentration of thermally-formed defect on Mg site
182 ($[V_{Mg}]^{intrinsic}$) is higher than impurity-formed Mg defect ($[V_{Mg}]^{extrinsic}$) in dry forsterite (here we
183 follow the Kröger and Vink (1956) notation for point defects, i.e., $[V_{Mg}]$ means the concentration
184 of defects on the Mg site).

185 The $[V_{Mg}]^{intrinsic}/[Mg_{Mg}^{\times}]$ ratio within the grain interior of dry forsterite is about 10^{-5} based on
186 thermogravimetric measurements (Tsai and Dieckmann, 2002). Namely, about 1 wt. ppm water
187 ($H^{+}/[Mg_{Mg}^{\times}] \approx 10^{-5}$) incorporated in the grain interior is enough to make $[V_{Mg}]^{extrinsic} > [V_{Mg}]^{intrinsic}$,
188 leading to an extrinsic mechanism for D_{Mg}^{lat} and therefore much lower ΔH_{Mg}^{lat} in hydrous
189 forsterite than dry condition (~280 kJ/mol vs. ~400 kJ/mol (Chakraborty et al., 1994; Fei et al.
190 2018)). On the other hand, $[V_{Mg}]^{intrinsic}$ in grain boundaries is expected to be much higher than the
191 $[V_{Mg}]^{intrinsic}$ within grain interiors due to lattice misfit (e.g., tilt and twist grain boundaries), namely,
192 $[V_{Mg}]^{intrinsic}/[Mg_{Mg}^{\times}] >> 10^{-5}$ on the grain boundaries of dry forsterite. Even though additional
193 extrinsic V_{Mg} are formed due to hydrogen incorporation, $[V_{Mg}]^{intrinsic} > [V_{Mg}]^{extrinsic}$ may still meet
194 on the grain boundaries. In this case, the grain-boundary diffusion of Mg in hydrous forsterite is
195 still dominated by intrinsic mechanism. In a summary, the above scenario suggests an intrinsic
196 mechanism for both D_{Mg}^{lat} and D_{Mg}^{gb} in dry forsterite, which explains the observed $\Delta H_{Mg}^{gb} \approx$
197 ΔH_{Mg}^{lat} (Chakraborty et al., 1994; Farver and Yund 1994), whereas in wet forsterite extrinsic and
198 intrinsic mechanisms dominate D_{Mg}^{lat} and D_{Mg}^{gb}, respectively, which leads to $\Delta H_{Mg}^{gb} >> \Delta H_{Mg}^{lat}$
199 (This study and Fei et al. 2018).

The cases of Si and O diffusion are different from that of Mg diffusion, because the concentrations of intrinsic V_{Si} and V_O are much lower than $[V_{Mg}]$ due to their high formation energy (Brodholt, 1997). Even small amounts of impurities (H^+, Fe^{3+}, Al^{3+}, and so on) may cause $[V_{Si}]^{extrinsic} >> [V_{Si}]^{intrinsic}$ and $[V_O]^{extrinsic} >> [V_O]^{intrinsic}$ both in the lattice and on the grain-boundaries, which suggests an extrinsic mechanism always dominate. As a result, the grain-boundary diffusion of both Si and O has lower activation energies than lattice diffusion, as experimentally determined (Farver and Yund, 2000; Fei et al. 2012, 2013, 2016; Shimojuku et al. 2009).

3.4 Water content dependence

So far there is no reported water content dependence of δD_{Mg}^{gb} in forsterite. Farver et al. (1994) compared the δD_{Mg}^{gb} in $H_2 + CO_2$ buffered and $CO + CO_2$ buffered samples, finding that the former is higher than the latter by a factor of ~6. Although they attributed this difference to enhancement by water in the $CO + CO_2$ buffered samples, they did not quantitatively analyze the water contents and therefore the water dependence of δD_{Mg}^{gb} remained unknown.

In this study, the samples with ~100-350 wt. ppm bulk water show significantly higher diffusivity than those with 20-30 wt. ppm bulk water and those measured by Farver et al. (1994) at ambient pressure, which should be extremely dry (Fig. 6). The least square fitting of data points from wet samples in Fig. 7 to Eqn. 3 suggests $r^{gb} = 1.0 \pm 0.1$, namely, δD_{Mg}^{gb} linearly increases with increasing Abs^{gb}. The value of r^{gb} is consistent with the linear relationship between $[V_{Mg}]$ and water fugacity (Kohlstedt, 2006). By assuming linear relationship between Abs^{gb} and bulk water content in grain boundaries ($C_{H2O}^{gb(bulk)}$), the effective bulk diffusivity contributed by grain-boundary diffusion is proportional to $C_{H2O}^{gb(bulk)}$, i.e.,

This is a preprint, the final version is subject to change, of the American Mineralogist (MSA)
Cite as Authors (Year) Title. American Mineralogist, in press.
DOI: https://doi.org/10.2138/am-2018-6480

$$D_{\mathrm{Mg}}{}^{\mathrm{gb(bulk)}} \propto \left(C_{\mathrm{H2O}}{}^{\mathrm{gb(bulk)}}\right)^{1.0\pm0.1} \quad (4)$$

since $D_{\mathrm{Mg}}{}^{\mathrm{gb(bulk)}} = 3\delta D_{\mathrm{Mg}}{}^{\mathrm{gb}}/d$ (Balluffi, 2005; Harrison, 1961; Kirchheim, 2001).

Comparing with Mg lattice diffusion, the water content exponent for $D_{\mathrm{Mg}}{}^{\mathrm{lat}}$ (r^{lat}) is 1.2 ± 0.2 (Fei et al. 2018), which is similar to r^{gb}. Namely, in contrast with the weak effect of water on Si and O diffusion (Fei et al., 2013, 2014, 2016), water has a major influence on Mg diffusion in forsterite both within the lattice and along the grain-boundaries. The slightly larger value of r^{lat} than that of r^{gb} may reflect the decrease in activation energy of the lattice diffusion by hydration.

3.5 Oxygen fugacity dependence

The f_{O2}-dependence experiments were performed at 1 atm, 1300 K in anhydrous forsterite. As shown in Fig. 8, even with f_{O2} increases from by 17.3 orders of magnitude, the $\delta D_{\mathrm{Mg}}{}^{\mathrm{gb}}$ appears to be nearly constant. The least square fitting gives,

$$\delta D_{\mathrm{Mg}}{}^{\mathrm{gb}} \propto (f_{\mathrm{O2}})^{-0.02\pm0.01} \quad (5)$$

Therefore, the grain-boundary diffusion of Mg in forsterite is insensitive to f_{O2}. This is identical to Mg lattice diffusion, which has $D_{\mathrm{Mg}}{}^{\mathrm{lat}} \propto (f_{\mathrm{O2}})^{0.01\pm0.01}$ (Fei et al. 2018).

In the view of point defect chemistry, the Mg diffusion rate should be proportional to $[V_{\mathrm{Mg}}]$. We have $[V_{\mathrm{Mg}}] \propto (f_{\mathrm{O2}})^{0}$ in forsterite based on the Schottky defect model (Smyth and Stocker, 1975). It leads to the no correlation between Mg diffusion and f_{O2}. Note that in the case of iron-bearing olivine, $[V_{\mathrm{Mg}}]$ increases with increasing f_{O2} with an exponent of 1/6 (Stocker and Smyth, 1978).

Therefore, the Mg diffusion coefficients in iron-bearing olivine are also expected to be f_{O2} dependent.

3.6 Implications

The effective bulk diffusivity of Mg, D_{Mg}^{bulk}, is defined by the summation of the lattice diffusion contribution and the grain-boundary diffusion contribution,

$$D_{\mathrm{Mg}}^{\mathrm{bulk}} = D_{\mathrm{Mg}}^{\mathrm{lat(bulk)}} + D_{\mathrm{Mg}}^{\mathrm{gb(bulk)}} \approx D_{\mathrm{Mg}}^{\mathrm{lat}} + \frac{3\delta}{d} D_{\mathrm{Mg}}^{\mathrm{gb}} \qquad (6)$$

The bulk diffusivity is dominated by lattice diffusion if $D_{Mg}^{lat} >> 3\delta D_{Mg}^{gb}/d$. In opposite, if $D_{Mg}^{lat} << 3\delta D_{Mg}^{gb}/d$, grain-boundary diffusion dominates. Our experimental results suggest that D_{Mg}^{lat} and δD_{Mg}^{gb} have almost identical pressure, water-content, and f_{O2} dependences, whereas the temperature effect on δD_{Mg}^{gb} is much larger than D_{Mg}^{lat} (this study and Fei et al., 2018)). Therefore, the dominance of the diffusion regimes is controlled by temperature and grain size.

A comparison of D_{Mg}^{lat} and $3\delta D_{Mg}^{gb}/d$ under various temperature and grain size conditions is shown in Fig. 9 at a pressure of 8 GPa and a bulk water content of 100 wt. ppm (typical water content in the upper mantle (Workman and Hart, 2005)). At temperatures of 1000 to 1800 K, we have $D_{Mg}^{lat} >> 3\delta D_{Mg}^{gb}/d$ if d > 1 mm. With decreasing grain size, $3\delta D_{Mg}^{gb}/d$ is significantly enhanced whereas D_{Mg}^{lat} is d-independent, and we have $D_{Mg}^{lat} \approx 3\delta D_{Mg}^{gb}/d$ when d = ~1 – 100 µm. When d << 1 µm, grain boundary diffusion will dominate since $D_{Mg}^{lat} << 3\delta D_{Mg}^{gb}/d$. In comparison with the grain size, temperature affects the relative magnitude of D_{Mg}^{lat} and $3\delta D_{Mg}^{gb}/d$ only slightly.

As we know, ionic electrical conduction of silicate minerals occurs by migration of charged ions. Since Mg is the fastest major elements diffusing in olivine (e.g., Chakraborty et al. 1994; Costa and Chakraborty, 2008), the ionic conductivity (σ_i) should be proportional to the Mg bulk diffusivity in olivine based on the Nernst-Einstein equation, $\sigma_i \propto D_{Mg}^{bulk}$. It suggests that in the Earth's asthenosphere, where the typical grain size is >1 mm (Faul and Jackson, 2005), the ionic conductivity of olivine is dominated by Mg lattice diffusion. In the case of subduction slabs, $D_{Mg}^{gb\ (bulk)}$ is significantly enhanced due to the much smaller grain sizes (1-100 μm (Wada et al. 2011)), as a result, $D_{Mg}^{gb\ (bulk)}$ and D_{Mg}^{lat} have comparable contribution to the ionic conductivity of olivine in slabs in spite of the relatively low temperature (Keken et al. 2002).

Acknowledgments:

We appreciate the help of Sumit Chakraborty and Ralf Dohmen at Ruhr-University Bochum for thin film deposition, and Chengcheng Zhao, Lin Wang, Esther Posner for discussions. We also thank Sylvie Demouchy and Ralf Milke for constructive comments. This work is funded by the Deutsche Forschungsgemeinschaft (DFG) to T. Katsura (KA3434/3-1, KA3434/7-1, KA3434/8-1, and KA3434/9-1), the Japan Society for the Promotion of Science (JSPS) to H. Fei (25003327), the JSPS KAKENHI Grant to H. Yurimoto (20002002), and the Earthquake Research Institute's cooperative research program. The TEM at BGI was financed by the DFG grant (No. INST 91/251-1 FUGG).

References:

Balluffi, R.W., Allen, S.M., and Carter, W.C. (2005) Kinetics of materials. John Wiley & Sons press, 645 pp.

Béjina, F., Blanchard, M., Wright, K., and Price, G.D. (2009) A computer simulation study of the effect of pressure on Mg diffusion in forsterite. Physics of the Earth and Planetary Interiors, 172, 13-19.

Brodholdt, J. (1997) Ab initio calculations on point defects in forsterite (Mg_2SiO_4) and implications for diffusion and creep. American Mineralogist, 82, 1049-1053.

Burnard, P., Demouchy, S., Delon, R., Arnaud, N.O., Marrocchi, Y., Cordier, P., Addad, A. (2015) The role of grain boundaries in the storage and transport of noble gases in the mantle. Earth and Planetary Science Letters, 430, 260-270.

Chakraborty, S., Farver, J.R., Yund, R.A., and Rubie, D.C. (1994) Mg trace diffusion in synthetic forsterite and San Carlos olivine as a function of *P*, *T*, and f_{O2}. Physics and Chemistry of Minerals, 21, 489-500.

Costa, F., and Chakraborty, S. (2008) The effect of water on Si and O diffusion rates in olivine and implications for transport properties and processes in the upper mantle. Physics of the Earth and Planetary Interiors, 166, 11-29.

Demouchy, S., Mackwell, S. (2006) Mechanisms of hydrogen incorporation and diffusion in iron-bearing olivine. Physics and Chemistry of Minerals, 33, 347-355.

295 Demouchy, S. (2010) Diffusion of hydrogen in olivine grain boundaries and implications for the
296 survival of water-rich zones in the Earth's mantle. Earth and Planetary Science Letters, 295,
297 305-313.

298 Dixon, J.E., Leist, L., Langmuir, C., and Schilling, J.G. (2002) Recycled dehydrated lithosphere
299 observed in plume-influenced mid-ocean-ridge basalt. Nature, 420, 385–389.

300 Farver, J.R., Yund, R.A., and Rubie, D.C. (1994) Magnesium grain boundary diffusion in forsterite
301 aggregates at 1000-1300 ^{o}C and 0.1 MPa to 10 GPa. Journal of Geophysical Research, 99,
302 19809-19819.

303 Farver, J.R., and Yund, R.A. (2000) Silicon diffusion in forsterite aggregates: implications for
304 diffusion accommodated creep. Geophysical Research Letters, 27, 2337-2340.

305 Faul, U.H., and Jackson, I. (2005) The seismological signature of temperature and grain size
306 variations in the upper mantle. Earth and Planetary Science Letters, 234, 119-134.

307 Fei, H., Hegoda, C., Yamazaki, D., Weidenbeck, M., Yurimoto, H., Shcheka, S., and Katsura, T.
308 (2012) High silicon self-diffusion coefficient in dry forsterite. Earth and Planetary Science
309 Letters, 345, 95-103.

310 Fei, H., Wiedenbeck, M., Yamazaki, D., and Katsura, T. (2013) Small effect of water on the upper
311 mantle rheology based on Si self-diffusion coefficient. Nature, 498, 213-215.

312 Fei, H., Wiedenbeck, M., Yamazaki, D., and Katsura, T. (2014) No effect of water on oxygen self-
313 diffusion rate in forsterite. Journal of Geophysical Research, 119, 7598-7606.

Fei, H., Koizumi, S., Sakamoto, N., Hashiguchi, M., Yurimoto, H., Marquardt, K., Miyajima, N., Yamazaki, D., and Katsura, T. (2016) New constraints on upper mantle creep mechanism inferred from silicon grain-boundary diffusion rates. Earth and Planetary Science Letters, 433, 350-359.

Fei, H., Koizumi, S., Sakamoto, N., Hashiguchi, M., Yurimoto, H., Marquardt, K., Miyajima, N., and Katsura, T. (2018) Mg lattice diffusion in iron-free olivine and implications to conductivity anomaly in the oceanic asthenosphere. Earth and Planetary Science Letters, 484, 204-212.

Harrison, L.G. (1961) Influence of dislocations on diffusion kinetics in solids with particular reference to the alkali halides. Transactions of the Faraday Society, 57, 1191–1199.

Hier-Majumder, S., Anderson, I.M., and Kohlstedt, D.L. (2005) Influence of protons on Fe-Mg interdiffusion in olivine. Journal of Geophysical Research 110, B02202.

Hiraga, T., Anderson, I.M., Zimmerman, M.E., Mei, S., and Kohlstedt, D.L. (2002) Structure and chemistry of grain boundaries in deformed, olivine + basalt and partially molten lherzolite aggregates: evidence of melt-free grain boundaries. Contributions to Mineralogy and Petrology, 144, 163-175.

Keken, P.E., Kiefer, B., and Peacock, S.M. (2002) High-resolution models of subduction zones: implications for mineral dehydration reactions and the transport of water into the deep mantle. Geochemistry Geophysics, Geosystems, 3, 1056, 1-20.

Keppler, H. and Rauch, M. (2000) Water solubility in nominally anhydrous minerals measured by FTIR and ^{1}H MAS NMR: the effect of sample preparation. Physics and Chemistry of Minerals, 27, 371-376.

Kirchheim, R. (2001). Solubility and diffusivity of hydrogen in complex materials. Physica Scripta, T94, 58-67.

Kohlstedt, D.L. (2006) The role of water in high-temperature rock deformation. Reviews in Mineralogy and Geochemistry, 62, 377-396.

Koizumi, S., Hiraga, T., Tachibana, C., Tasaka, M., Miyazaki, T., Kobayashi, T., Takamasa, A., Ohashi, N., and Sano, S. (2010) Synthesis of high dense and fine-grained aggregates of mantle composites by vacuum sintering of nano-sized mineral powders. Physics and Chemistry of Minerals, 37, 505-518.

Kröger, F.A., and Vink, H.J. (1956) Relations between the concentrations of imperfections in crystalline solids. Solid State Physics, 3, 307-435.

Marquardt, K., Rohrer, G.S., Morales, L., Rybacki, E., Marquardt H., and Lin B. (2015) The most frequent interfaces in olivine aggregates: the GBCD and its importance for grain boundary related processes. Contributions to Mineralogy and Petrology, 170, 40. Doi: 10.1007/s00410-015-1193-9.

Marquardt, K. and Faul, U.H. (2018) The structure and composition of olivine grain boundaries: 40 years of studies, status and current developments. Physics and Chemistry of Minerals, 45, 139-172.

Ringwood, A.E. (1991) Phase-transformations and their bearing on the constitution and dynamics of the mantle. Geochimica et Cosmochimica Acta, 55, 2083-2110.

Shimojuku, A., Kubo, T., Ohtani, E., Nakamura, T., Okazaki, R., Dohmen, R., and Chakraborty, S. (2009) Si and O diffusion in $(Mg,Fe)_2SiO_4$ wadsleyite and ringwoodite and its implications for the rheology of the mantle transition zone. Earth and Planetary Science Letters, 284, 103-112.

Smyth, D.M., and Stocker, R.L. (1975) Point defects and non-stoichiometry in forsterite. Physics of the Earth and Planetary Interiors, 10, 183-192.

Stocker, R.L., and Smyth, D.M. (1978) Effect of enstatite activity and oxygen partial pressure on the point-defect chemistry of olivine. Physics of the Earth and Planetary Interiors, 16, 145-156.

Tsai, T.L., and Dieckmann, R. (2002) Variation of the oxygen content and point defects in olivines, $Fe_xMg_{1-x})_2SiO_4$, $0.2 \leq x \leq 1.0$. Physics and Chemistry of Minerals, 29, 680-694.

Wada, I., Behn, M.D., and He, J.H. (2011) Grain-size distribution in the mantle wedge of subduction zones. Journal of Geophysical Research, 116, B10203.

Wang, Z.Y., Hiraga, T., and Kohlstedt, D.L. (2004) Effect of H^+ on Fe-Mg interdiffusion in olivine, $(Fe,Mg)_2SiO_4$. Applied Physics Letters 85, 209-211.

Withers, A.C., Bureau, H., Raepsaet, C., and Hirschmann, M.M. (2012) Calibration of infrared spectroscopy by elastic recoil detection analysis of H in synthetic olivine. Chemical Geology, 334, 92-98.

Workman, R.K., and Hart, S.R. (2005) Major and trace element composition of the depleted MORB mantle (DMM). Earth and Planetary Science Letters, 231, 53-72.

Figure captions:

Fig. 1. SEM and TEM images of the recovered samples taken with acceleration voltages of 30 and 200 kV, respectively. The TEM images were taken with defocus between Scherzer (for maximum resolution) and 0 defocus. (a) Secondary electron image of dry sample (D7). (b) Secondary electron image of wet sample (V760). (c) Original high resolution TEM image of dry sample (D7). (d) Original high resolution TEM image of wet sample (H3667).

Fig. 2. Examples of FTIR spectra after baseline correction and thickness normalization to 1 cm showing different bulk water contents in the samples. (a) The sharp peaks at 3613, 3579, 3550, 3568, and 3473 cm^{-1} are assigned to be grain interior OH, whereas the broad bands are assumed to be grain boundary water. The infrared absorptions by grain boundary OH are obtained by integration of the broad bands from 4000 to 3000 cm^{-1}. (b) After deconvolution of the peaks at 3613, 3579, 3550, 3568, and 3473 cm^{-1}, the infrared absorptions by grain boundary OH are obtained by integration of the residual spectra.

Fig. 3. Examples of diffusion profiles under dry and wet conditions (D18B and V760#1, respectively). The lattice and grain-boundary diffusion regimes appeared in the shallow and deeper parts of the profiles, respectively. The δD_{Mg}^{gb} were obtained by fitting the grain-boundary diffusion regimes to Eqn. (1).

Fig. 4. δD_{Mg}^{gb} in the samples annealed under the same pressure, temperature, water content, and oxygen fugacity conditions, but with different durations.

Fig. 5. Pressure dependence of δD_{Mg}^{gb} at 1300 K in anhydrous forsterite in comparison with that reported by Farver et al. (1994). At low pressure conditions, the δD_{Mg}^{gb} determined in this study is identical with that by Farver et al. (1994). However, with increasing pressure, the absolute values of δD_{Mg}^{gb} measured in this study is much lower.

Fig. 6. Temperature dependence of δD_{Mg}^{gb} at 8 GPa in comparison with that determined by Farver et al. (1994). Note that the data reported by Farver et al. (1994) is recalculated to 8 GPa using the ΔE_{Mg}^{gb} reported in this study. Farver et al. (1994) reported the activation energy (ΔE_{Mg}^{gb}) of 343 ± 27 and 376 ± 47 kJ/mol for CO + CO_2 and H_2 + CO_2 buffered samples, respectively. The activation enthalpy (ΔH_{Mg}^{gb}) becomes 370 – 410 kJ/mol with the pressure correction to 8 GPa using the activation volume determined in this study. The high-pressure data points by Farver et al. (1994) is not shown here because we do not know their water contents.

Fig. 7. Water content (total infrared absorption contributed by grain boundary OH) dependence of δD_{Mg}^{gb} at 8 GPa, 1100 - 1300 K. (a) Abs^{gb} is calculated based on the method given in Fig. 2a. (b) Abs^{gb} is calculated based on the method given in Fig. 2b.

Fig. 8. f_{O2} dependence of δD_{Mg}^{gb} at 1 atm, 1300 K in anhydrous forsterite with f_{O2} in the range of 10^{-18} – $10^{-0.7}$ bar. No meaningful correlation between δD_{Mg}^{gb} and f_{O2} was found.

Fig. 9. Effective grain-boundary diffusivity ($D_{Mg}^{gb(bulk)} = 3\delta D_{Mg}^{gb}/d$) and lattice diffusivity (D_{Mg}^{lat}) in forsterite under various grain size and temperature conditions at 8 GPa and bulk water content of 100 wt. ppm by assuming δ = 1 nm (Hiraga et al., 2002).

Table 1

A list of experimental conditions and fitting results of δD_{Mg}^{gb}. The run numbers #1, #2, and #3 indicate different profiles obtained from the same sample.

Run. No.	*P* (GPa)	*T* (K)	*t* (h)	*d* (μm)	(talc+brucite): graphite (volume ratio)	C_{H2O}^{bulk} (wt.ppm)[*a]	Abs^{gb} (cm^{-2})		δD_{Mg}^{gb}
							Broad band[*b]	Deconvolution residual[*c]	(m^3/s)
V756#1	8	1100	16	0.6	1:10	273	1550	1131±157	3.9×10^{-26}
V756#2	8	1100	16	0.6	1:10	273	1550	1131±157	2.5×10^{-26}
V758#1	8	1200	2	0.6	1:20	198	1125	830±257	2.2×10^{-24}
V758#2	8	1200	2	0.6	1:20	198	1125	830±257	1.0×10^{-24}
V758#3	8	1200	2	0.6	1:20	198	1125	830±257	6.5×10^{-25}
S5752	8	1200	30	0.6	1:40	20	55	28±22	4.8×10^{-26}
V797T	8	1200	30	0.6	1:20	106	587	344±253	2.6×10^{-25}
V797M*[d]	8	1200	30	2	1:40	26	130	101±56	3.4×10^{-25}
H3670#1	8	1200	3	0.6	1:20	98	588	444±129	7.7×10^{-25}
H3670#2	8	1200	3	0.6	1:20	98	588	444±129	7.3×10^{-25}
V760#1	8	1300	0.5	0.6	1:10	350	1768	1477±415	2.2×10^{-23}
V760#2	8	1300	0.5	0.6	1:10	350	1768	1477±415	1.0×10^{-23}
H3679#1	8	1300	1	0.6	1:40	20	43	58±12	8.5×10^{-25}
H3679#2	8	1300	1	0.6	1:40	20	43	58±12	5.4×10^{-25}
H3679#3	8	1300	1	0.6	1:40	20	43	58±12	2.9×10^{-25}
H3734	8	1300	10	0.6	1:40	32	140	113±29	7.7×10^{-25}
H3667#1	8	1300	2	0.6	1:20	130	704	568±141	1.1×10^{-23}
H3667#2	8	1300	2	0.6	1:20	130	704	568±141	8.6×10^{-24}
H3699	8	1300	10	2	C_{H2O}^{bulk} < 1 wt.ppm				1.9×10^{-25}
S5746	8	1300	30	2					1.7×10^{-25}
V798	1	1300	9	0.6					1.3×10^{-24}
V789	4	1300	9	0.6					2.1×10^{-25}
H3749#1	13	1300	9	0.6					1.0×10^{-26}
H3749#2	13	1300	9	0.6					1.5×10^{-26}
D21	1 atm	1300	22.2	0.6	Dry, $\log f_{O2}$ (bar) = -10.5				3.5×10^{-24}
D22		1300	6	0.6	Dry, $\log f_{O2}$ (bar) = -10.5				1.7×10^{-24}
D23		1300	40.2	0.6	Dry, $\log f_{O2}$ (bar) = -10.5				1.0×10^{-24}
D7		1300	3	0.6	Dry, $\log f_{O2}$ (bar) = -10.5				1.3×10^{-24}
D24		1300	9	0.6	Dry, $\log f_{O2}$ (bar) = -5.0				2.1×10^{-24}
D25		1300	11	0.6	Dry, $\log f_{O2}$ (bar) = -18.0				1.2×10^{-24}
D18B		1300	16	0.6	Dry, $\log f_{O2}$ (bar) = -15.0				3.2×10^{-24}
D12S		1300	4	0.6	Dry, $\log f_{O2}$ (bar) = -0.7				7.2×10^{-25}
D12L		1300	4	2	Dry, $\log f_{O2}$ (bar) = -0.7				8.8×10^{-25}

*a. The bulk water content is calculated from the total infrared absorptions (both grain boundary and grain interior OH in Fig. 2a) using Withers et al. (2012)'s calibration by assuming the same absorption coefficient for lattice and grain boundary OH in iron-bearing olivine (Fo90) and pure forsterite (Fo100).

*b. Abs^{gb} calculated by integration of the broad bands of the FTIR spectra from 3000 to 4000 cm^{-1} as shown in Fig. 2a.

*c. Abs^{gb} calculated by integration of the residual of FTIR spectra from 3000 to 4000 cm^{-1} after deconvolution of the sharp peaks at 3613, 3579, 3568, 3550, 3473 cm^{-1} as shown in Fig. 2b. The error bars of Abs^{gb} are also given since deconvolution process always produces large uncertainty.

*d. The sample V797T is not used for the determination of ΔH_{Mg}^{gb} and r^{gb} since it has larger grain size than other samples.

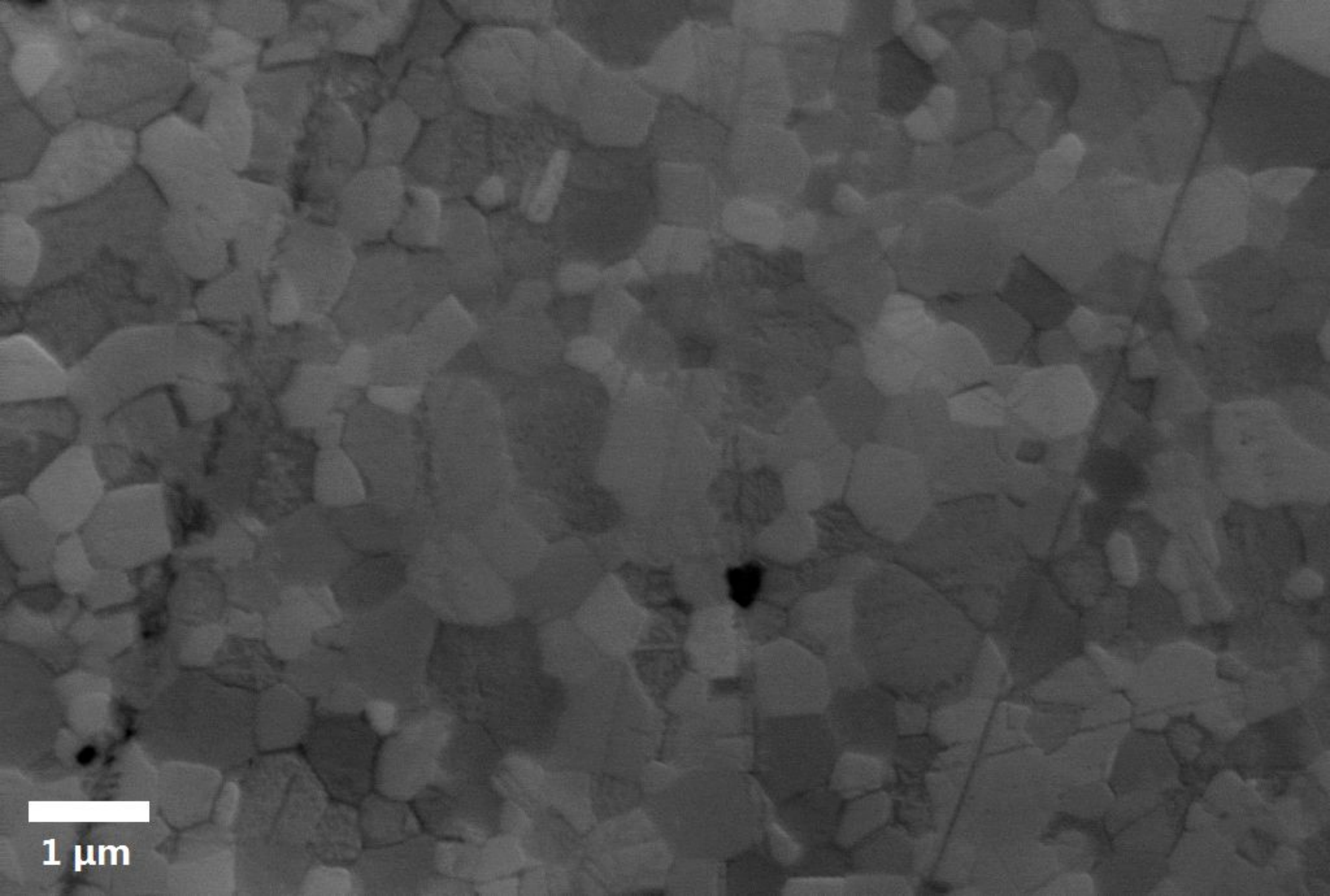
1 µm

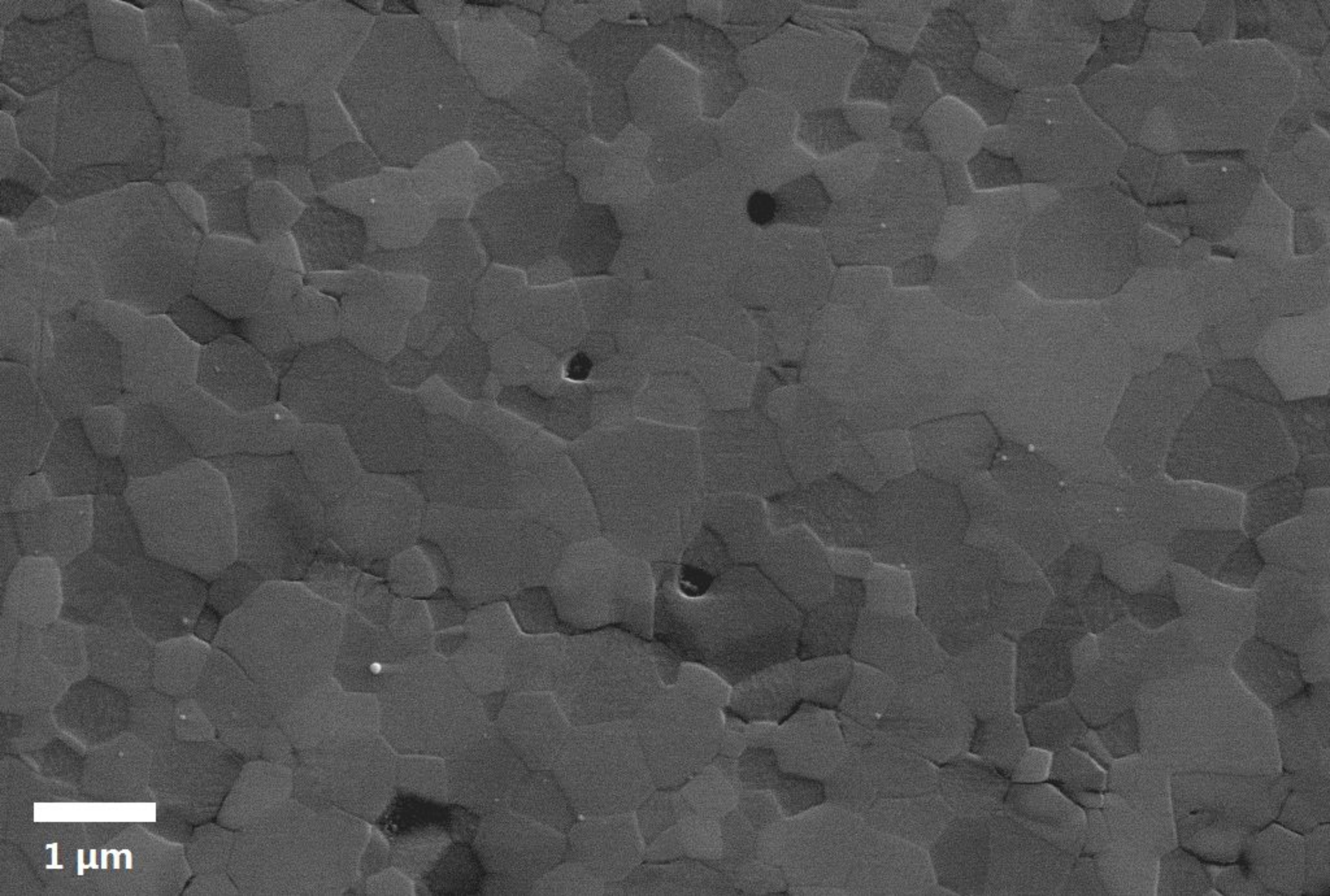
1 µm

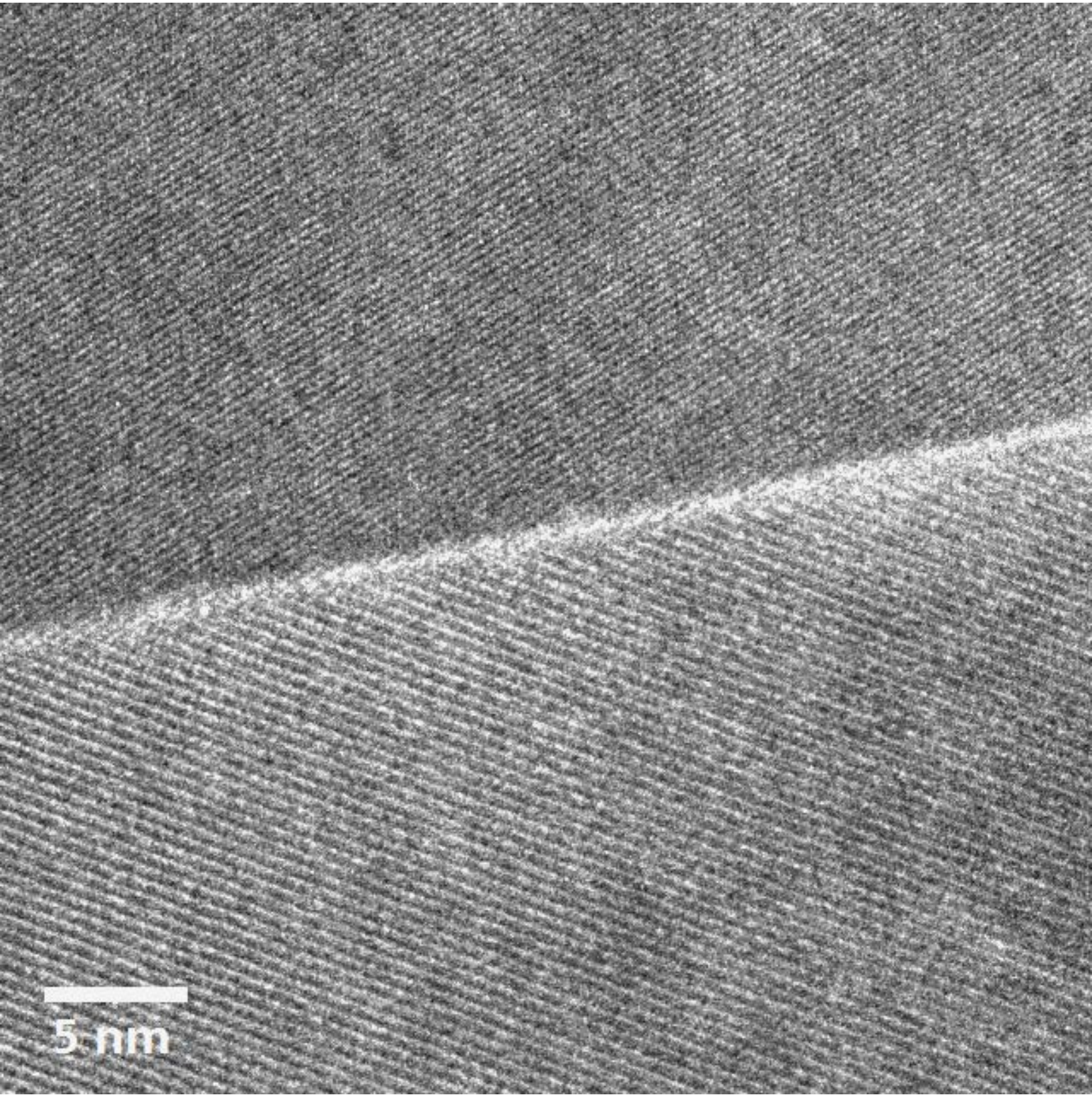
5 nm

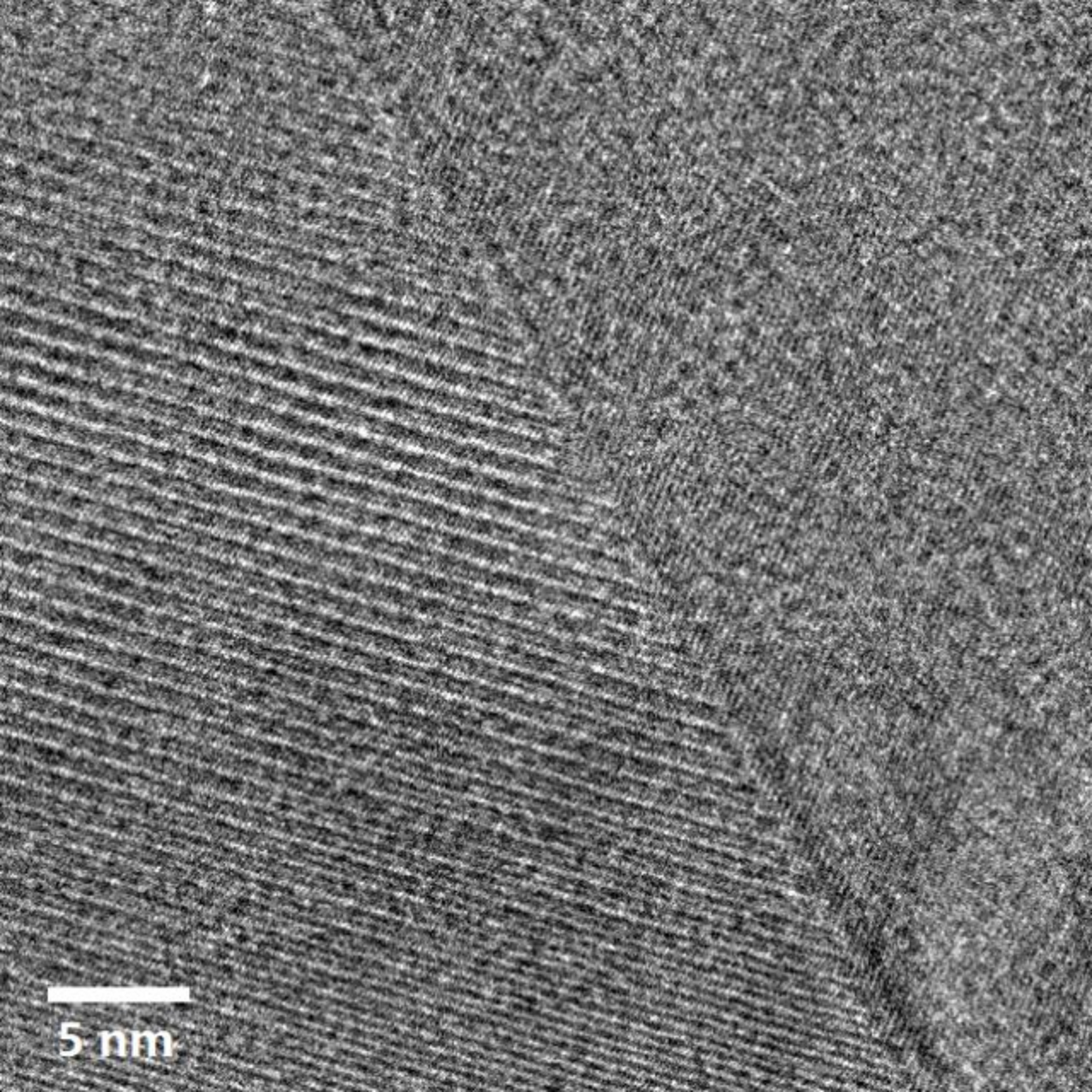
5 nm

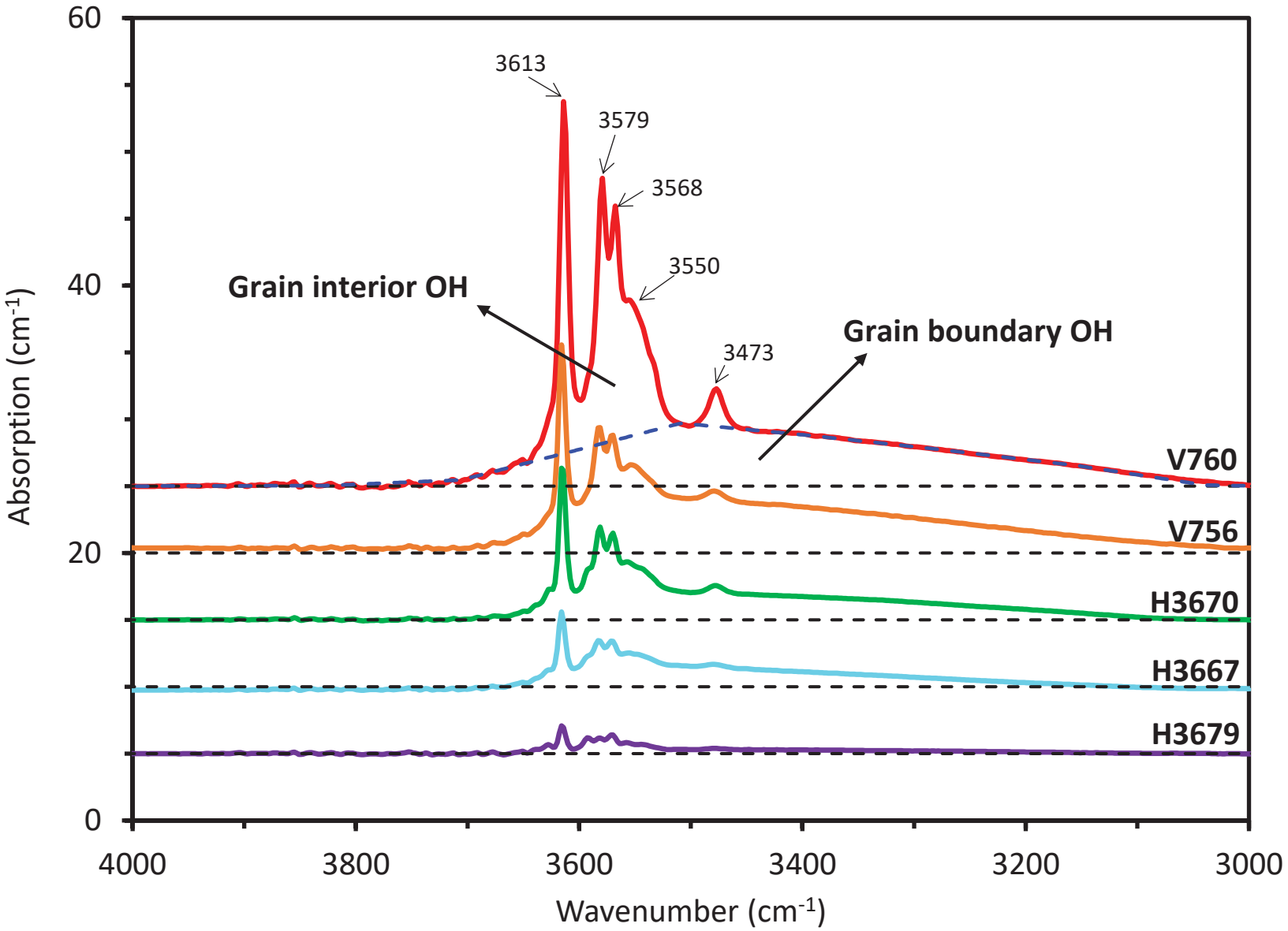
60
40
20
0
Absorption (cm-1)
3613
3579
3568
3550
3473
Grain interior OH
Grain boundary OH
V760
V756
H3670
H3667
H3679
4000
3800
3600
3400
3200
3000
Wavenumber (cm-1)

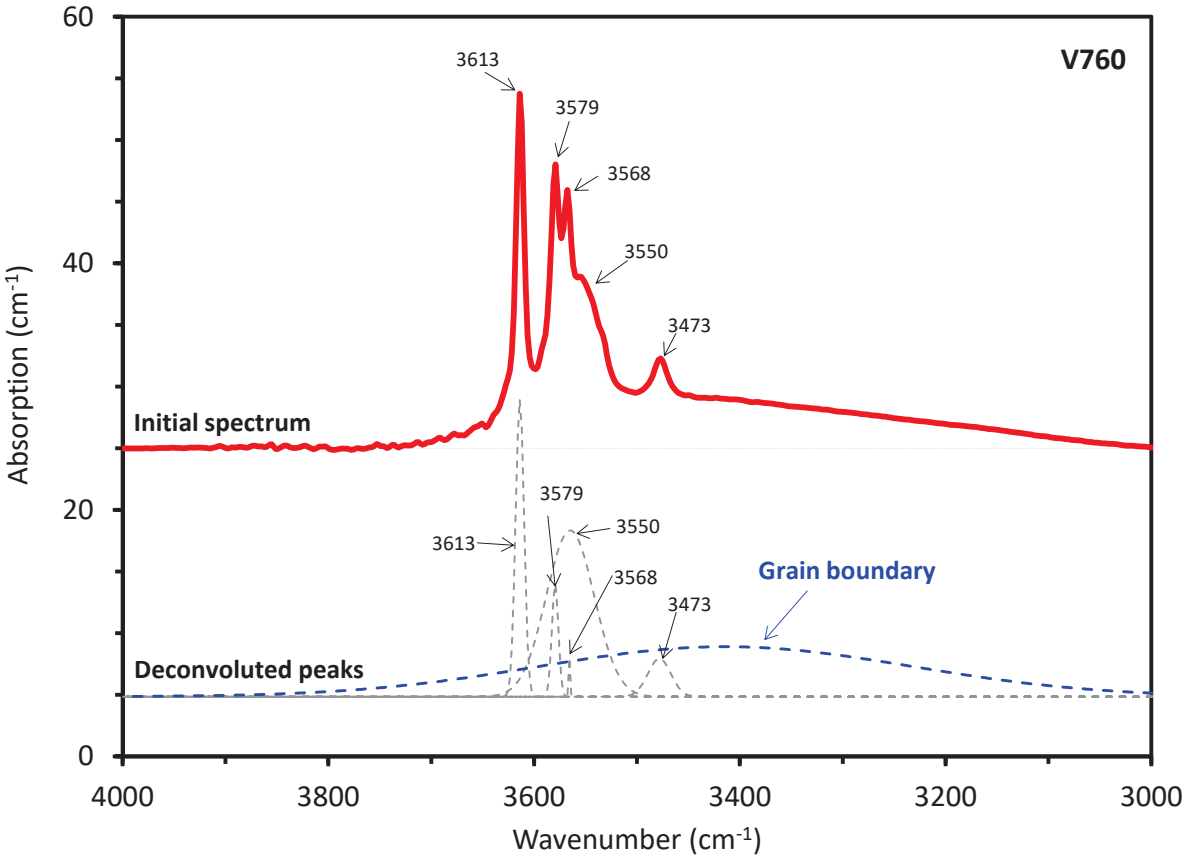
V760
3613
3579
3568
3550
3473
Initial spectrum
Deconvoluted peaks
Grain boundary
Absorption (cm-1)
Wavenumber (cm-1)
60
40
20
0
4000
3800
3600
3400
3200
3000

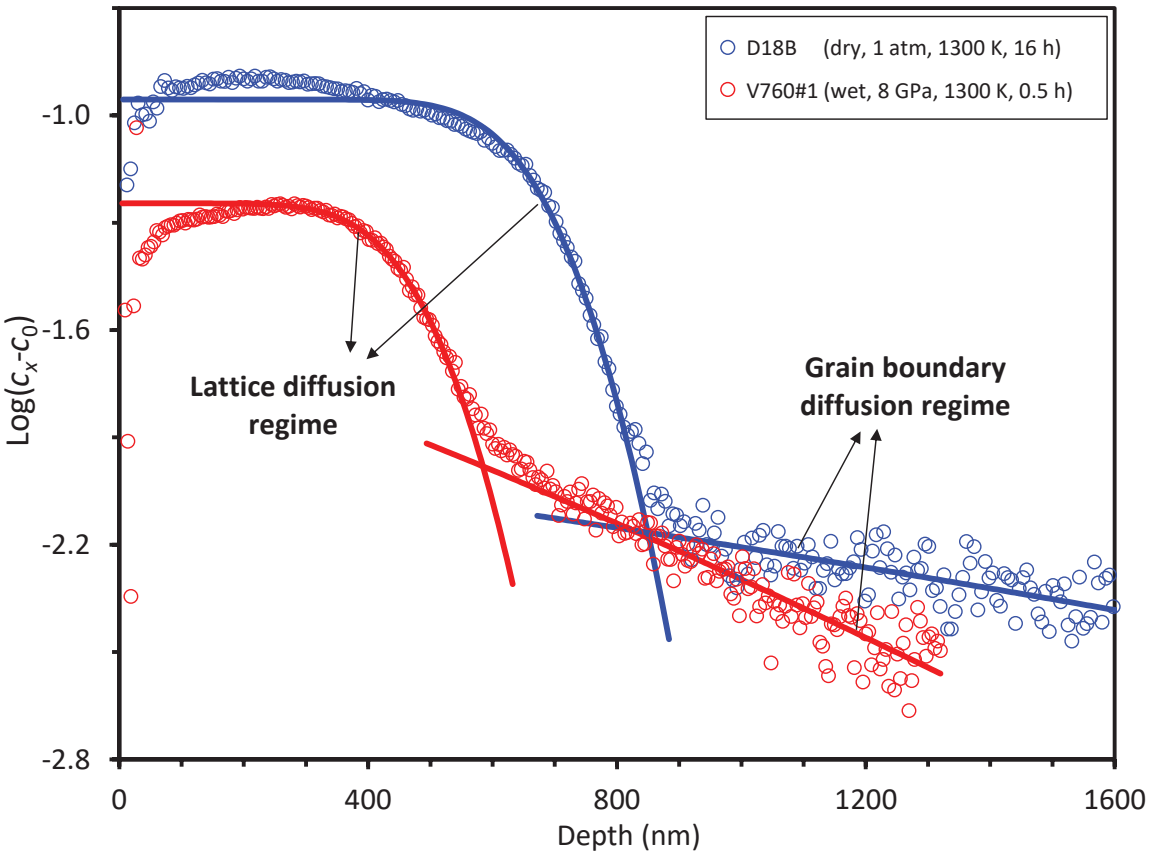
D18B (dry, 1 atm, 1300 K, 16 h)
V760#1 (wet, 8 GPa, 1300 K, 0.5 h)
Lattice diffusion regime
Grain boundary diffusion regime
Log(c_x-c_0)
-1.0
-1.6
-2.2
-2.8
0
400
800
1200
1600
Depth (nm)

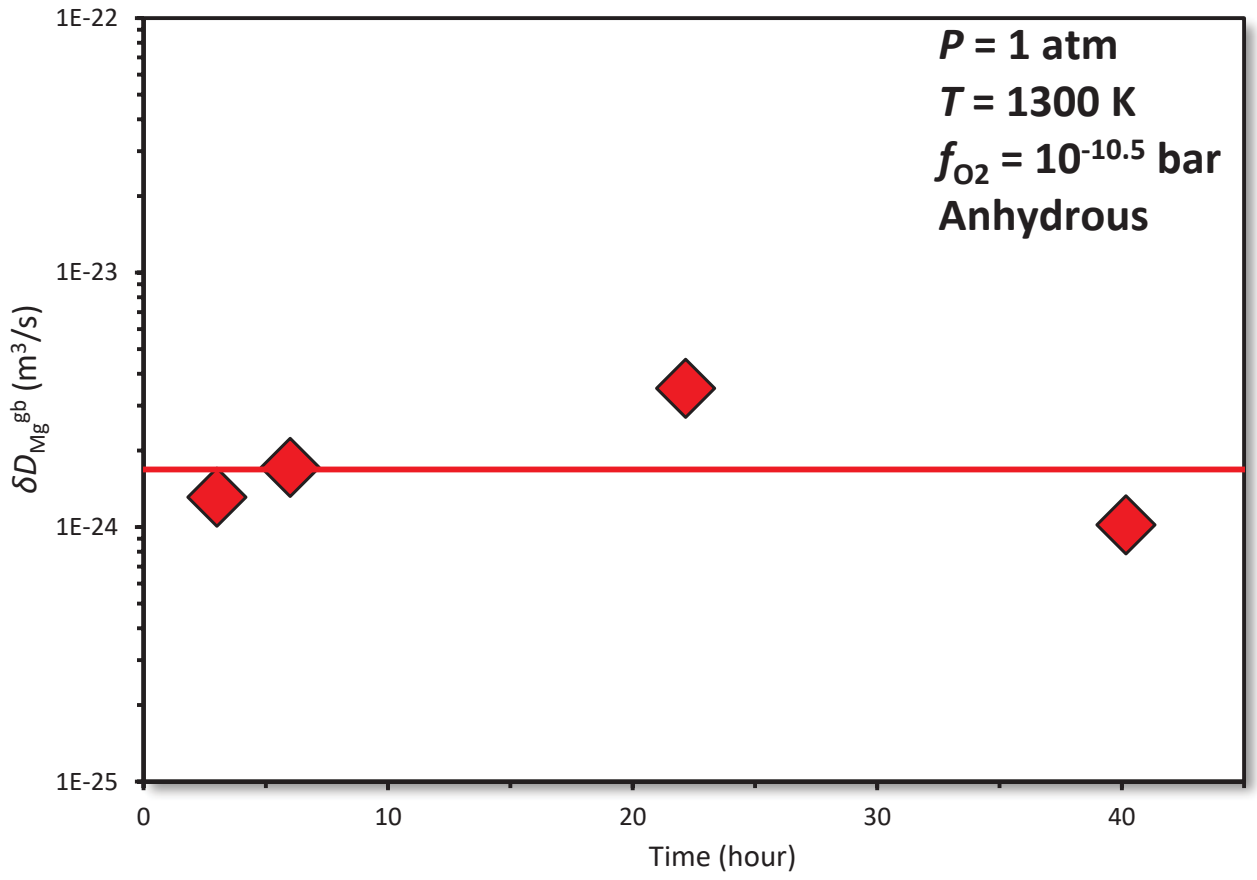
P = 1 atm
T = 1300 K
f_{O2} = $10^{-10.5}$ bar
Anhydrous
1E-22
1E-23
1E-24
1E-25
δD_{Mg}^{gb} (m^3/s)
0
10
20
30
40
Time (hour)

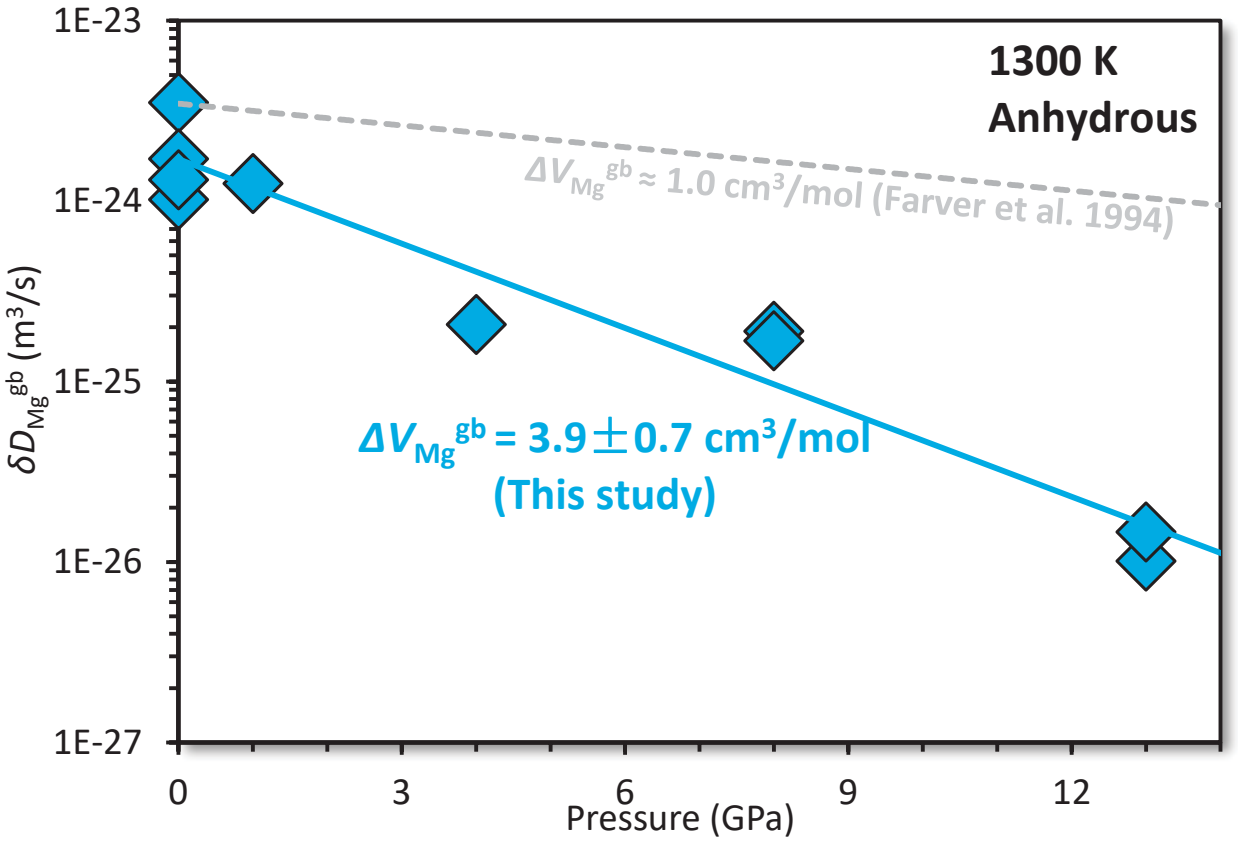
1E-23
1E-24
1E-25
1E-26
1E-27
δD_{Mg}^{gb} (m^3/s)
0
3
6
9
12
Pressure (GPa)
1300 K
Anhydrous
$\Delta V_{Mg}^{gb} \approx 1.0$ cm^3/mol (Farver et al. 1994)
$\Delta V_{Mg}^{gb} = 3.9 \pm 0.7$ cm^3/mol
(This study)

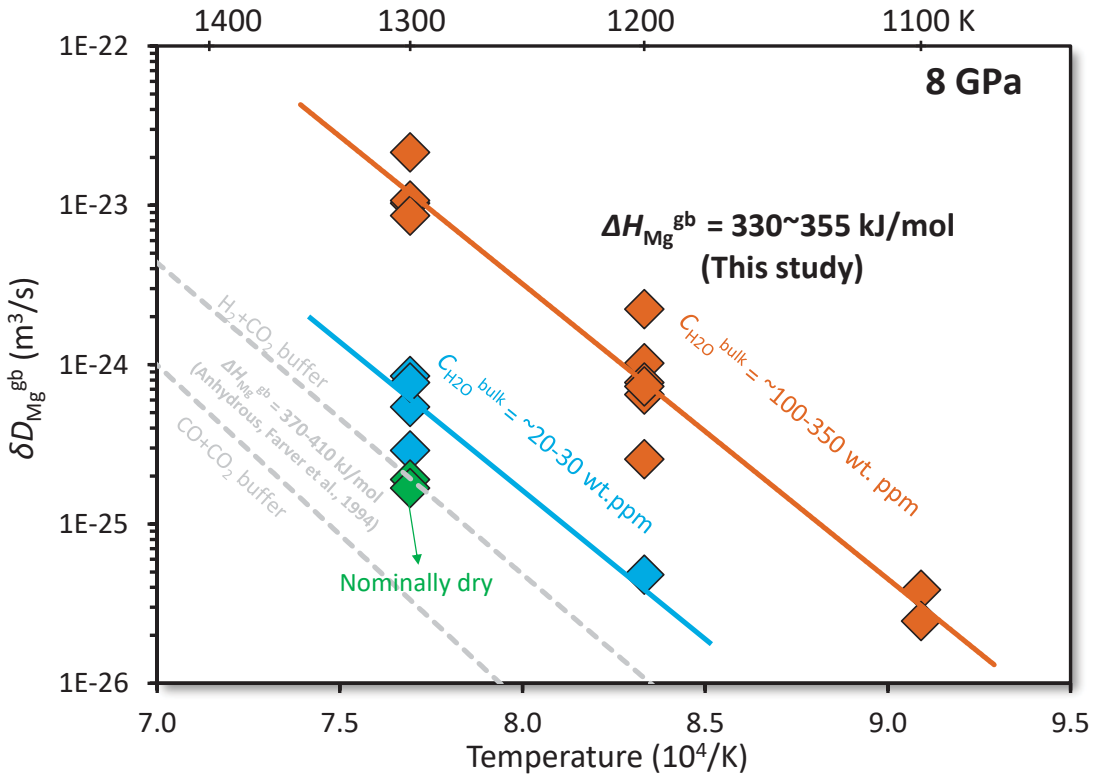
1400
1300
1200
1100 K
1E-22
1E-23
1E-24
1E-25
1E-26
8 GPa
ΔH_{Mg}^{gb} = 330~355 kJ/mol
(This study)
C_{H2O} bulk = ~100-350 wt. ppm
C_{H2O} bulk = ~20-30 wt.ppm
H_2+CO_2 buffer
ΔH_{Mg}^{gb} = 370-410 kJ/mol
(Anhydrous, Farver et al., 1994)
CO+CO_2 buffer
Nominally dry
δD_{Mg}^{gb} (m^3/s)
7.0
7.5
8.0
8.5
9.0
9.5
Temperature (10^4/K)

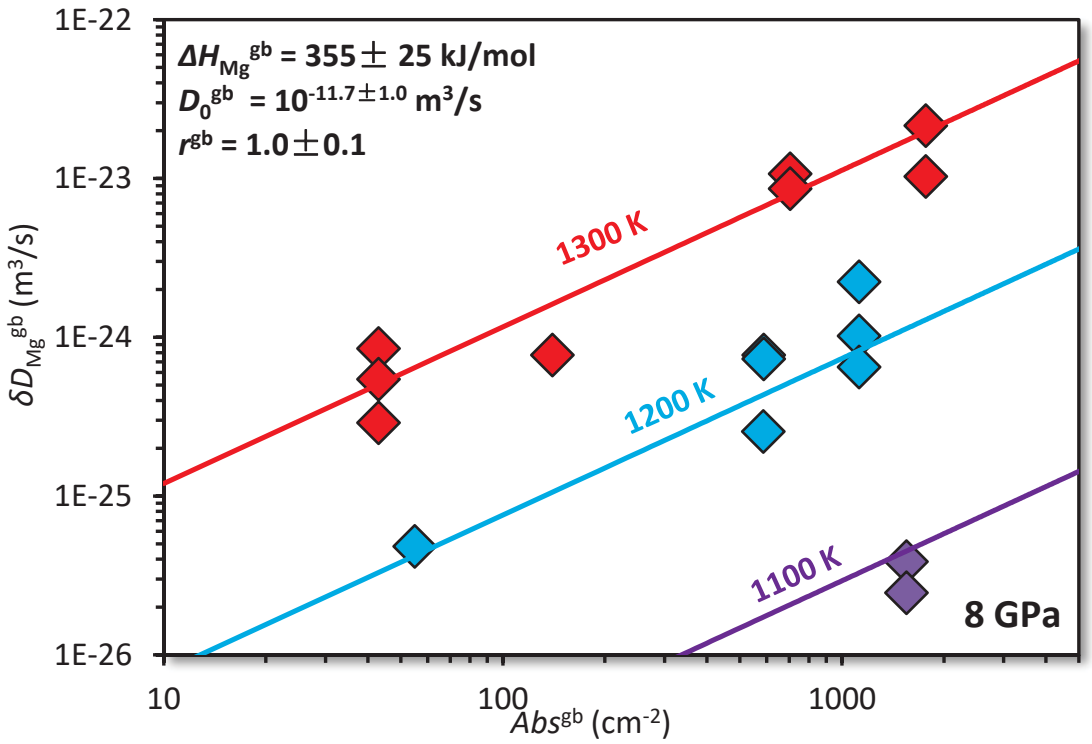
ΔH_{Mg}^{gb} = 355 ± 25 kJ/mol
D_0^{gb} = $10^{-11.7 \pm 1.0}$ m³/s
r^{gb} = 1.0 ± 0.1
1300 K
1200 K
1100 K
8 GPa
1E-22
1E-23
1E-24
1E-25
1E-26
δD_{Mg}^{gb} (m³/s)
10
100
1000
Abs^{gb} (cm^{-2})

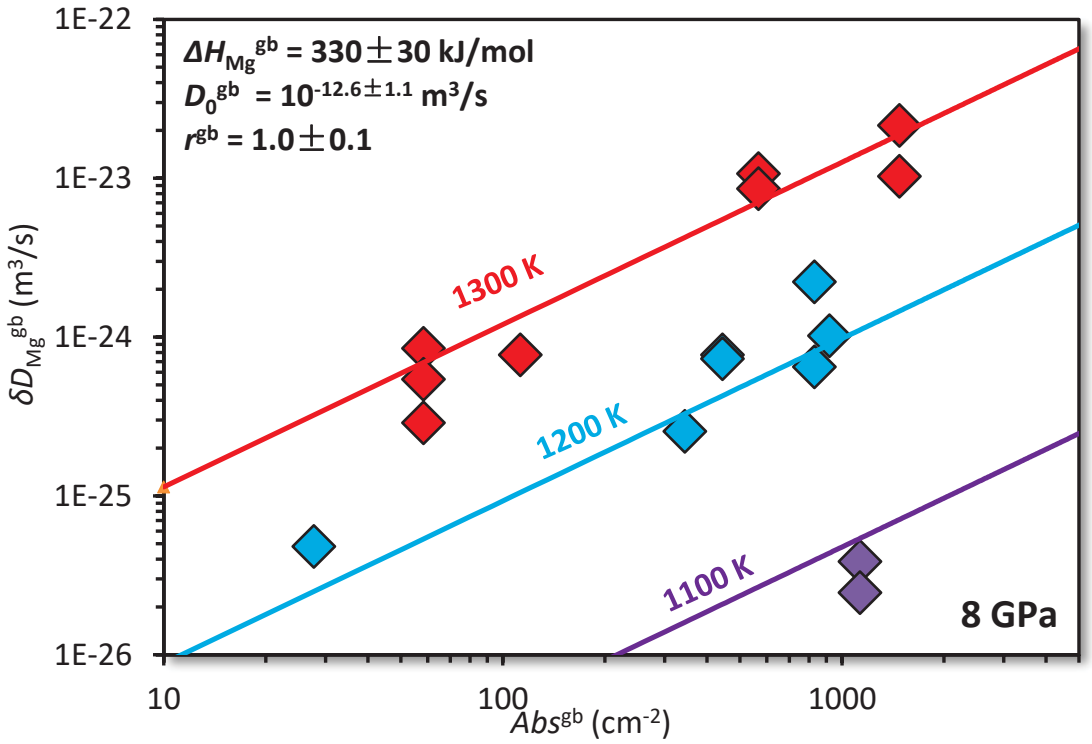
ΔH_{Mg}^{gb} = 330±30 kJ/mol
D_0^{gb} = $10^{-12.6\pm1.1}$ m³/s
r^{gb} = 1.0±0.1
1300 K
1200 K
1100 K
8 GPa
1E-22
1E-23
1E-24
1E-25
1E-26
δD_{Mg}^{gb} (m³/s)
10
100
1000
Abs^{gb} (cm^{-2})

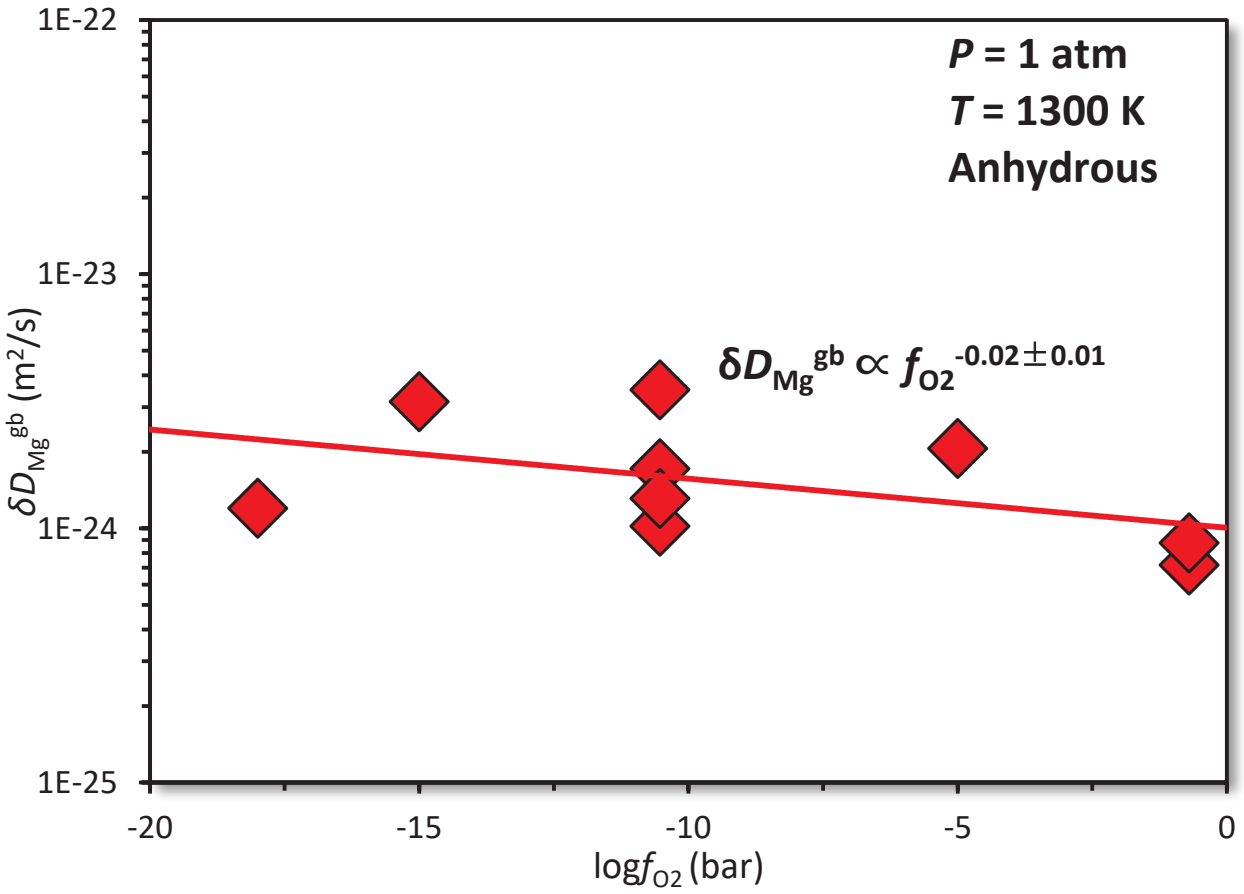
1E-22
1E-23
1E-24
1E-25
δD_{Mg}^{gb} (m^2/s)
-20
-15
-10
-5
0
logf_{O2} (bar)
P = 1 atm
T = 1300 K
Anhydrous
$\delta D_{Mg}^{gb} \propto f_{O2}^{-0.02\pm0.01}$

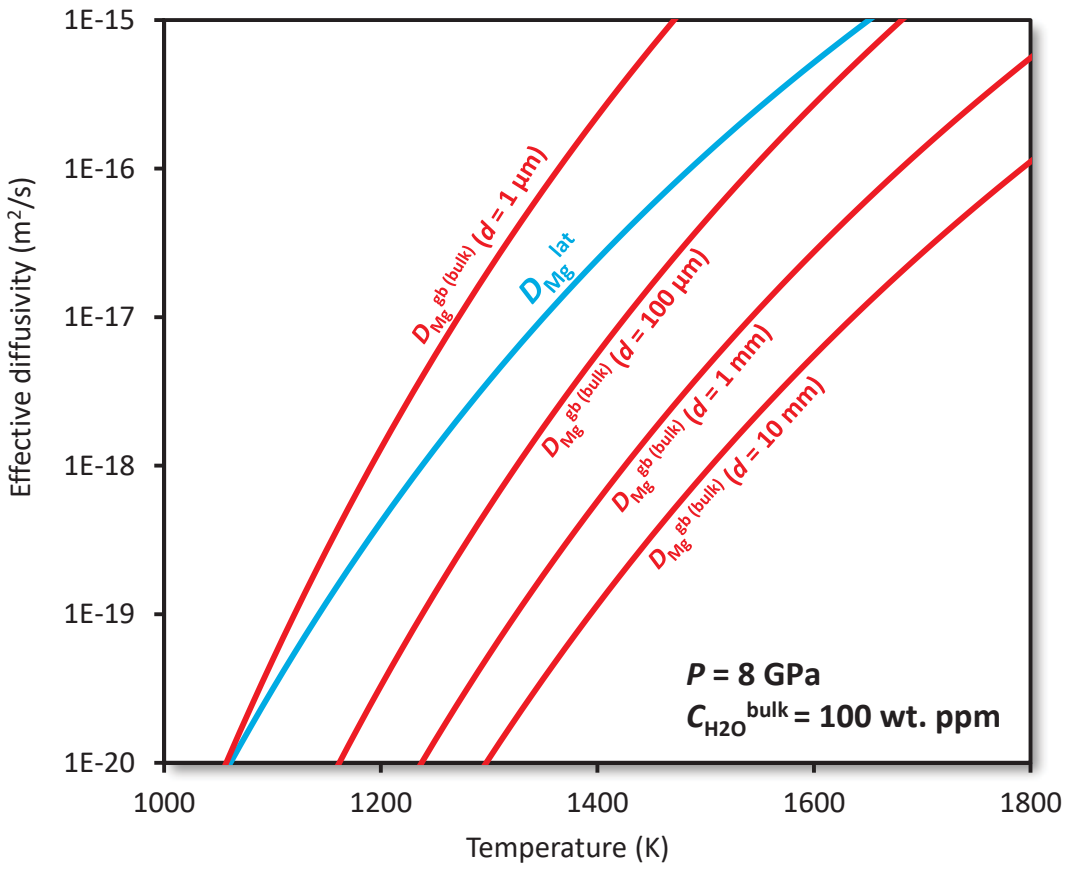
1E-15
1E-16
1E-17
1E-18
1E-19
1E-20
Effective diffusivity (m²/s)
1000
1200
1400
1600
1800
Temperature (K)
D_Mg gb (bulk) (d = 1 µm)
D_Mg lat
D_Mg gb (bulk) (d = 100 µm)
D_Mg gb (bulk) (d = 1 mm)
D_Mg gb (bulk) (d = 10 mm)
P = 8 GPa
C_H2O bulk = 100 wt. ppm